Ultrasonic Bulk Wave Measurements on Composite using Fiber from Recycled CFRP

David Patereson[1, a)], Winifred L Ijomah[1], James FC Windmill[2], Chih-Chuan Kao[1], Grant Smillie[2]

1 Design, Manufacture, and Engineering Management, University of Strathclyde, 75 Montrose St, Glasgow, United Kingdom, G1 1XJ
2 Dept. of Electronic and Electrical Engineering, University of Strathclyde, 204 George Street, Glasgow, United Kingdom, G1 1XW.

a) Corresponding author: David.a.Paterson@Strath.ac.uk

Abstract. This study investigates the velocity profile for both a virgin carbon fiber reinforced plastic (v-CFRP) and a reused fiber CFRP (rf-CFRP) which exhibit quasi-isotropy; all samples have 3 iterations of symmetry type $[0, -45, +45, 90]_s$. An isotropic virgin CFRP (v-CFRP), produced by using a hand layup process, is presented along with a pyrolysis recycling process (at 600^{o}C) designed to extract the carbon fibers. A virgin carbon fiber mat with a similar architecture was also thermally conditioned under the same pyrolysis conditions. Both resultant carbon fiber mats were used to produce the rf-CFRPs. Ultrasonic wave velocities at different angles of incidence for both v-CFRP and rf-CFRP were recorded. In the case of v-CFRP, two samples were studied and it was recorded that the velocity for both a longitudinal wave and transverse wave remained relatively constant up until these waves completely attenuated at observed angles, indicating what would be expected from an isotropic sample. A close relationship in terms of waves speed was also recorded for the two v-CFRP samples. In the case of rf-CFRP, the longitudinal wave velocities were generally less closely related when compared to the v-CFRP, with a maximum of approximately 32% difference being recorded. The transverse wave velocity was also found to decrease incident angle indicating sample anisotropy. The authors suggest that the more severe decreasing velocity with increasing incident angle, when compared to v-CFRP, may be caused by resin impregnation issues and not by changes that occur during the recycling process. Therefore, a hypothesis that both the rf-CFRP and the V-CFRP will return a similar wave profile given an identical resin fiber content is put forward.

1.0 INTRODUCTION

The study of bulk wave propagation via immersion based ultrasonic velocity measurements has received significant attention within literature, with areas such as frequency selection, the anisotropy of the sample, sample rotation, wave direction, symmetry plane analysis, critical angle evaluation, group velocity wave deviation all being investigated [1–6]. However, almost all literature is concerned with v-CFRP only; no literature to the authors' knowledge exists which investigates if bulk wave propagation follows the same pattern of wave propagation when propagating in rf-CFRP - CFRP manufactured using fibers from a virgin CFRP that has undergone a recycling process [7]. Note this material is also commonly referred to as recycled CFRP in literature [8–12].

This work will seek to investigate this area and conduct wave velocity measurements on quasi-isotropic CFRP with 3 iterations of layup $[0, -45, +45, 90]_s$. First, an identification as to why wave velocity measurements are conducted is put forward. Following this, an experimental section outlining the composite creation process for both v-CFRP and rf-CFRP is documented along with like for like ultrasonic wave propagation analysis on both v-CFRP and rf-CFRP. Lastly, a discussion section evaluating the results obtained for rf-CFRP and v-CFRP is presented alongside a conclusion.

1.1 Relationship Between Velocity and Elastic Constants

Typically when determining material properties such as ultimate tensile strength, Young's modulus, shear Modulus and Poisson ratio the experiments tend to be destructive and often require particular shaped parts [10,13]. These material parameters all depend on the elastic constants of a material, which through wave propagation are able to be determined non-destructively. Consequently elastic wave propagation is and has been for some time a common method to determine the elastic constants of materials; the relationship between the phase velocity and the elastic constants is through the Christoffel equation [1–3,5,6,14–18].

For propagation in an isotropic material, noting that the composite used in this research is quasi-isotropic, equations 1-3 outline phase velocity elastic constant relationships.

$$v_x = \sqrt{C_{44}/\rho} \tag{1}$$

$$v_y = \sqrt{C_{44}/\rho} \tag{2}$$

$$v_z = \sqrt{C_{11}/\rho} \tag{3}$$

Where, the subscript x, y or z, identifies the direction of wave polarization for waves propagating in given direction. The symbol ρ is the density of the material, and is calculated by dividing the mass by the volume.

2.0 EXPERIMENTAL METHOD

2.1 v-CFRP Manufacture

24 square Toray T300 unidirectional carbon fiber samples of 18 cm by 18 cm were excised from a standard 1m by 1m roll. Of these 24 samples, 6 had the fiber direction 0^o, 6 had the fiber direction 90^o, 6 had the fiber direction -45^o and 6 had the fiber direction $+45^o$. Figure 1 is given to reinforce this concept

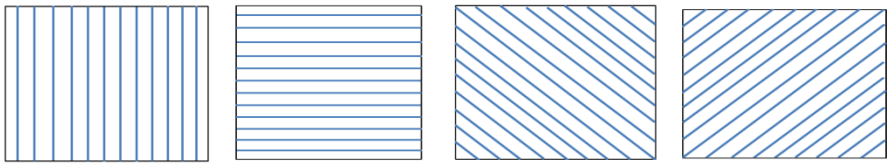

(a) (b) (c) (d)

FIGURE 1. Figure (a) documents fiber direction of 0^o to the top edge, (b) documents 90^o, (c) documents -45^o and (d) documents $+45^o$

The manufacturing process was by hand layering as follows. First, a flat piece of metal was coated in a polyvinyl alcohol (PVA) mould release agent with the first square fiber mat of 0^o placed upon it. A degassed resin hardener solution mixed to specification of 100:30 was poured over the sample. The second fiber mat of -45^o was then placed up the 0^o sample, with baking paper placed over the -45^o sample. A 50mm bristled roller was then rolled over the samples to ensure both compactness and an even spread of resin between the two fiber layers. Further resin was poured on the -45^o sample with a similar process being carried out until the composite had 24 layers. At this stage, a large heavier flat piece of metal, coated in release agent was placed onto the top layer. The structure was placed inside a fume extractor hood and left in situ for 48 hours, with a heavier weight placed upon the top metal layer. The resultant composite was 4mm thick. All materials were purchased from Easycomposite.co.uk noting that the resin was EL2 epoxy with slow hardener

At this point the composite was hard and rigid and thus suitable for further mechanical treatment. From this larger section of composite, two samples of approximately $36cm^2$ (6cm by 6cm) were machined using a Roland

EGX-600 CNC router. These samples are v-CFRP A and v-CFRP B. Note that due to an error occurring during preparation, the 5th layer, which according to the sequence should have been set to 90^0 was set to 0^0 instead.

2.2 Pyrolysis Recycling Process

The pyrolysis process performed was in keeping with that reported in literature, [8–11,19,20] A standard Carbolite oven was preheated for approximately 1 hour until the figure of 600^0C was reached. The samples were allowed to dwell for 45 minutes and then were removed and allowed to cool in ambient air.

The temperature was chosen in accordance with Meyer et al.[20] who documented that at 600 ^{0}C epoxy resin would have gone through a full pyrolysis process resulting in complete oxidation. Further, Meyer et al. [20] also documented that the carbon fiber is general not affected by oxidation at 600^0C – note these results document only the epoxy resin and carbon fibers in isolation. The authors also identify that for pyrolysis of CFRP at 600^0C, oxidization of the carbon fibers will increase with increased dwelling times. Striking a balance to fully remove the resin and leave the fibers largely intact, a time period of 45 minutes was selected, in accordance with results outlined in [20].

The sections of v-CFRP placed inside the oven were not the 6cm by 6cm samples, instead smaller sections of v-CFRP, excised from the larger original (18cm by 18 cm) v-CFRP were used instead.

2.3 Simulated Pyrolysis Recycling Process

To simulate the recycling process, smaller hand laid up samples of carbon fiber were heat treated under the same conditions as previously outlined for the recycling of v-CFRP. Similar to the v-CFRP, the hand laid up structures used in simulated pyrolysis were $36cm^2$ (6cm by 6cm) of similar fiber architecture.

2.4 Production of rf-CFRP

After the thermal process and the fibers returned to ambient temperature, the fibers were carefully placed onto a metal plate (coated in PVA mould release agent), to ensure the architecture of the fiber mats originating from the pyrolysis and simulated recycled process was maintained. However, with the thermal process degrading the protective netting covering the fibers, the fiber layers were not able to be manipulated by hand. Therefore, unlike the hand-layup process, the degassed 100:30 mixed resin hardener solution was poured evenly over the top layer of the fiber mat before a second piece of metal was placed on top of the fibers with a weight being placed upon the metal plate. The composite was left in situ again for 48 hours.

A variety of different composites were created at this point. Unlike the v-CFRP creation process, an output of the rf-CFRP manufacturing process was that an oval shape of partially impregnated region in the centre of each sample was recorded. Thus, available sections of fully cured and impregnated simulated rf-CFRP were manually excised from around these oval regions. 8 rf-CFRP samples, referenced as A1 – D2, were used in this study. Table 1 outlines the fiber mats used for these rf-CFRP samples.

TABLE 1. Outlining the rf-samples and the types of fiber mat used to create them. A1 and A2 are created using mats from true pyrolysis with B1-D2 using mats from simulated pyrolysis.

Recycling Process	Samples							
	A1	A2	B1	B2	C1	C2	D1	D2
True Recycling	*	*						
Simulated Recycling			*	*	*	*	*	*

2.5 Ultrasonic Velocity Measurements

The velocity measurements were performed using an immersion based ultrasonic through transmission method [2,3]. Figure 2 (a) and (b) identify the experimental arrangement used for this study.

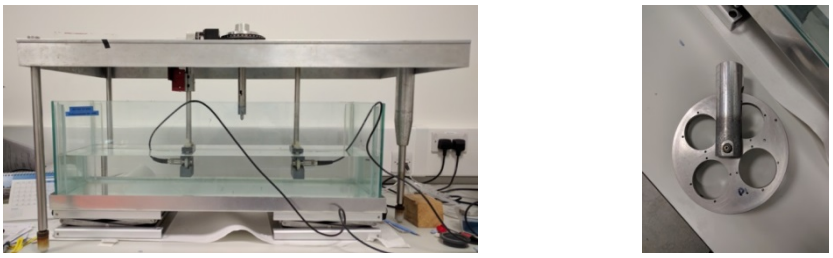

(a) (b)

FIGURE 2. Figure (a) shows both the emitting and receiving transducers, immersed in a body of oil. Figure (b) shows the mechanical rotation device, controlled mechanically from above, upon which the samples were placed. In this research, the samples were not circular and were housed across the slots and not housed within the slots.

An ultrasonic signal was transmitted from transducer A and recorded by transducer B. The transducers frequency was 2.25 MHz with a voltage of 10V peak-to-peak. The transducer separation distance was 289.55mm (sample placed directly between both transducers) with the coupling medium being Perfluoropolyether oil –PFPE.

The longitudinal velocity was recorded by ensonifying the samples at a normal with respect to the emitting transducer. To record the transverse wave velocity, the sample was rotated horizontally (from the transducer's perspective) and via mode conversion, a transverse wave was generated and propagated through the sample. To understand the degree of isotropy which existed in the sample, the sample was continually rotated until after the second critical angle (the shear critical angle) was apparent. For an isotropic sample, transverse velocity will remain constant up until the critical angle is reached, at which point, the incident wave is totally reflected.

The velocity was recorded using a correlation method [21], and rearranging equations (1 – 3) allowed for the elastic constants to be determined.

3.0 EXPERIMENTAL RESULTS

3.1 v-CFRP

The reference wave velocity (no sample between transducers) was recorded as 662.8 m/s. The samples were weighed using digital scales accurate to one decimal point, with the volume calculated geometrically. Table 2 provides density, weight, volume and % error for the v-CFRP samples.

TABLE 2 – Documenting the volume, weight and density values for v-CFRP samples A and B. The % error between samples is also shown.

Data	v-CFRP A	v-CFRP B	% Error
Volume	14.4 cm^3	14.4 cm^3	0%
Weight	19.0 g	18.6 g	2.1%
Density	1319.444 kg/m^{-3}	1291.667 kgm^{-3}	2.1%

Initially, both samples were subjected to ultrasonic wave propagation at normal incidence, i.e. 0^0. Both samples at this point were then subsequently rotated to investigate critical angles. Investigating the first critical angle sample A and sample B were rotated towards the theoretical predicted critical angle (calculated using the velocity at 0^0) of approximately 16^0. At this point the critical angle was not easily observable owing to what was believed to be the early emergence of a transverse wave alongside the decaying longitudinal wave. Moving past the 16^0 degrees mark, the output signal featured only a transverse element.

The second critical angle was able to be accurately observed and was found to be 32^0 in both samples, with the estimated critical angle based on velocity at maximum amplitude found to be 29.94^0 and 30.01^0 degrees respectively. Investigating this further, from approximately 20^0 - critical angle velocity, sample A and sample B recorded a % difference in transverse wave velocity of approximately 10.7% and 17.6%. Thus, while quasi-isotropy

is assumed, the velocity decrease indicates that the samples are not perfectly quasi-isotropic – particularly as the critical angle was approached. In terms of velocity change with increasing incident angle for the longitudinal waves, the % difference figures were lower and were recorded as 6.57% and 3.5% for sample A and B respectively.

In terms of like for like wave velocity measurements, the % error for a longitudinal wave incident at 0^0 in samples A and B was approximately 2% which upon taking into account possible inaccuracy arising from experimental error and fiber orientation errors in the hand lay-up process, is very reasonable. A similar measurement was taken at values of maximum amplitude for the transverse waves and found to be even more closely related than the longitudinal waves, with a value of around 0.2% being recorded.

Moving onto the elastic constants, equations 1-3 were used to determine C11 and C44, with small % error being recorded between the samples. These results along with key data recorded for the v-CFRP samples are given in table 3, with velocity profile and amplitude profile against incident angle for sample A given as figure 3.

TABLE 3. Data recorded for the v-CFRP samples. Small % errors were recorded between the samples, indicating a strong degree of homogeneity in the larger samples used to create both A and B.

Data	Sample A	Sample B	% difference between samples
Longitudinal wave speed (m/s)	2439	2382.3	2.35%
Transverse wave speed (m/s)	1327.7	1325	0.2%.
First critical angle (**practical**)	N/A	N/A	N/A
First critical angle (**theoretical**)	15.77^0	16.15^0	2.38%
Second critical angle (**practical**)	32.0^0	32.0^0	0%
Second critical angle (**theoretical**)	29.94^0	30.01^0	0.23%
C_{11}	7.85 GPa	7.33 GPa	6.85%
C_{44}	2.32 GPa	2.26 GPa	2.62%

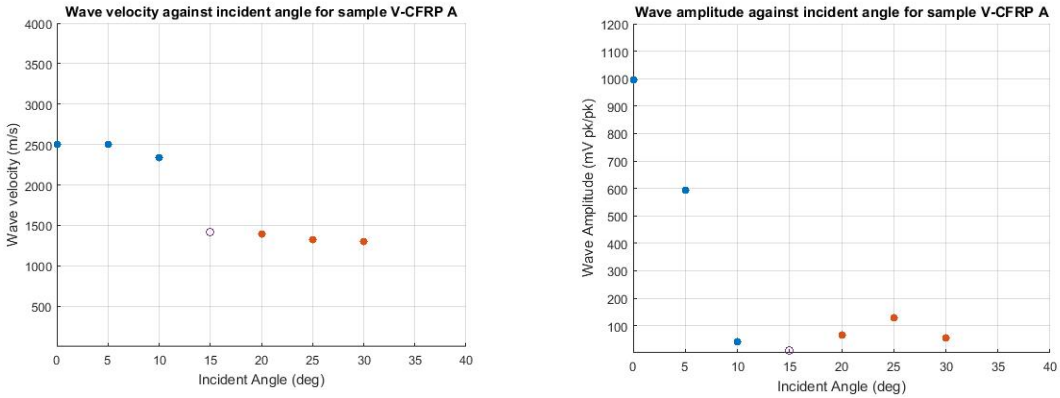

(a) (b)

FIGURE 3. Figure a) outlines the longitudinal and transverse wave propagation against incident angle for sample v-CFRP A. Between 0 and 10 there was a 6.3% change in longitudinal velocity recorded, between angles of 20 and 30 there was a 6.6% change in transverse velocity. The hollow point the wave recorded as the longitudinal decays and the transverse builds, the velocity recorded (1413m/s) is more in keeping with the expected transverse velocity, giving rise to the belief that the wave was more transverse than longitudinal. Figure b) documents the amplitude against incident angle showing a decaying longitudinal wave with an emerging transverse wave, with a critical angle in keeping with prediction.

3.2 Rf-CFRP

Samples A1 – D2 were all subject to the same ultrasonic testing as outlined for the v-CFRP. In this instance, a reference voltage was taken 5 times, once for each class of sample (i.e. once for A, once for B, etc.). The initial reference velocity was recorded as 662.5 m/s and the subsequent reference velocities recorded stayed with 0.5% of this value.

At 0^0 incidence % errors of approximately 32%, 30%, 8%, 20% in longitudinal wave velocity was recorded between samples A1 and A2, B1 and B2, C1 and C2, and D1 and D2 respectively. With such differences in velocity, non-identical resin / CF content between the samples was inferred. Further, the % error in density between the samples was recorded as 6.35%, 11.72%, 5.31% and 7.60% respectively.

Investigating the first critical angle, with regards to A1 and A2 (the samples created through true recycling), the longitudinal waves was found to quickly attenuate around the 6^0 incident mark, with the emergence of a transverse wave recorded earlier than that for v-CFRP. For samples B1, B2, C1, C2 and D1, this phenomenon was recorded at around 5^0, while for sample D2 it was recorded at 8.5^0. In all cases and similar to the v-CFRP samples, the exact critical angle was difficult to conclusively observe. However, the transverse wave did start to independently emerge in all cases between 10 - 15^0, which for the large part is in keeping with theoretical predictions using a longitudinal velocity figure at 0^0 incidence (see table 4).

An exceptional case is noted for sample D1 and D2; owing to the relatively large longitudinal velocity figures recorded when compared to samples A1, A2, B1, B2, and C1 and C2, the critical angle was forecast at a lower value of around 5 degrees. Figure 4 a) and b) document the wave amplitude against incident angle for samples A2 and B1

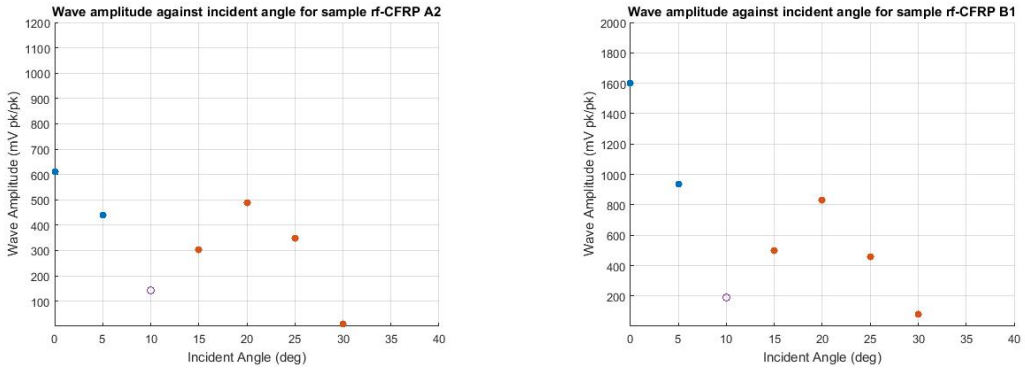

(a) (b)

FIGURE 4. Figure a) and b) document the wave amplitude against incident angle for samples rf-CFRP A2 and B1. Close agreement in terms of amplitude profile is found between the figures and with that recorded in figure 3 (b). Similar to figure 3, note the hollow point. The wave profile in this region coincides with an emerging shear wave and decaying longitudinal wave.

Investigating now the second critical angle, the wave profile recorded for all samples differed from that recorded with the v-CFRP. Rotating the rf-CFRP samples towards the second critical angle it was found that the wave velocity steadily decreased as the critical angle was approached, more so than in the case for the v-CFRP. While the % difference between the v-CFRP transverse velocity at 20^0 and critical angle velocity was found to be 10.7% and 17.6% for samples v-CFRP A and B, for the rf-CFRP samples, the % difference varied between approximately 21 – 33%.

The second critical angle for all rf-CFRP samples was observed, with values ranging from approximately 29-32^0. This critical angle is in keeping with the v-CFRP case, and suggests a fair degree of sample homogeneity in terms of architecture between both the rf-CFRP samples themselves and between the rf-CFRP samples and the v-CFRP samples. A velocity measurement was taken at maximum signal amplitude for all the samples, and to highlight the decreasing velocity with increasing incident angle another velocity measurement was taken (if applicable i.e. attenuation was not significant) between the maximum amplitude value and the critical angle. These

velocities are recorded in table 4. A full wave profile recorded for rf-CFRP samples A2 and B1, outlining the above wave profile is given in figures 5 a) and b). Note that owing to correlation problems the wave velocity at 10^0 was not able to be recorded for B1.

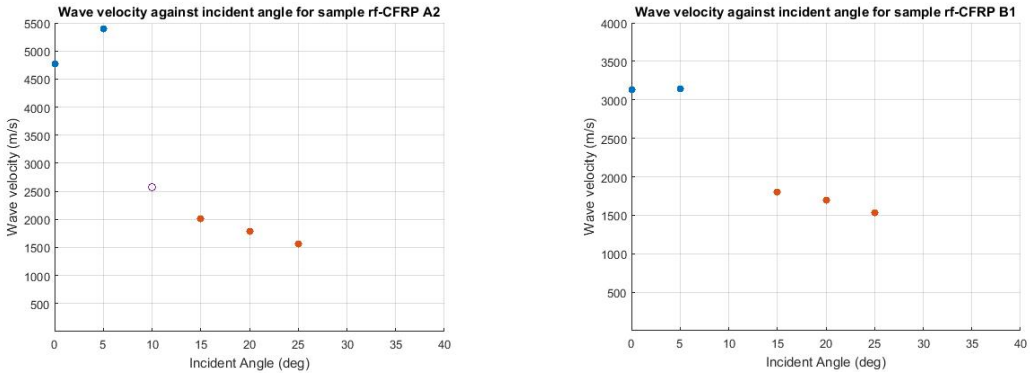

(a) (b)

FIGURE 5. Figure a) and b) show the wave velocity against incident angle for rf-CFRP samples A2 and B1. The longitudinal velocity for A1 increases sharply by 11% then decays, noting again the hollow point. B1 longitudinal velocity remains relatively constant. For both samples, the transverse velocity is decreasing with increasing incident angle, between 15 and 25 degrees there is a velocity change of 22% and 15% respectively, which is significant when compared with changes of wave velocity of 6.6% in the case of v-CFRP A (figure 4).

It should be noted that with sample C1 an exception to the above was found. In this sample, a longitudinal wave was found to decay with a transverse wave emerging and then quickly attenuating at around 13.5^0. At this point, a transverse wave emerges again and follows the same propagation pattern as the other samples.

It can also be noted from figures 5 a) and b) that the wave velocity at the critical angle is not recorded while table 4 also outlines some velocity values that were not able to be recorded, for instance C1 and D2. The velocity was unable to be recorded in these cases due to a combination of attenuation, sample size and transducer width. Concerning the difficulty in recording the velocity at the critical angles, as the critical angle was approached the sample width was less than transducer width and so the receiving transducer recorded not only the transverse wave velocity but also the velocity at which the wave propagated through the coupling medium at either side of the sample.

Normally this is not a problem, however, owing to the attenuation recorded within the samples, signal correlation problems were evident. Highlighting the wave profile recorded when the oil and sample velocities are merged together, figure 6 is presented.

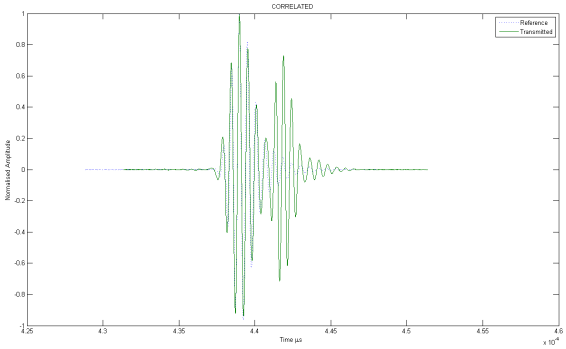

FIGURE 6. Correlated image of transverse wave (incident at 26^{o}) and reference wave for sample A1. The first peak is the transverse wave, the second peak is the reference wave from the oil. If the transverse wave amplitude attenuates below the reference wave, correlation problems start to occur.

With the critical angle able to be visually observed for every sample however, a theoretical prediction of the transverse wave velocity at this angle was able to be made. These velocities, along with the relevant information for each sample is again given in table 4. Note additionally, due to a non-constant wave velocity, equations 1-3 would return inaccurate elastic constants and so these parameters were not determined for the rf-CFRP samples.

TABLE 4. Wave phenomenon recorded for the rf-CFRP samples. L: and T indicate longitudinal and transverse wave respectively and N/A identifies that a measurement was not able to take place.

Data	A1	A2	% diff	B1	B2	% diff	C1	C2	% diff	D1	D1	% diff
L wave speed (m/s)	3073.3	4245	32.02	3103.9	4228.6	30.69	3459.2	3189.3	8.12	7437.2	6031.2	20.88
Max-amp T wave speed (m/s) (incident angle)	1679.1 (21^{o})	1667.8 (23^{o})	0.67	1765.5 (20^{o})	1778.3 (21^{o})	0.72	N/A	1736.9 (21^{o})	N/A	1623 (24^{o})	N/A	N/A
T wave speed (m/s) between (Max-amp) transverse and critical angle (incident angle)	1495.4 (26^{o})	1458.2 (27^{o})	2.52	1633.4 (23^{o})	N/A (25^{o})	N/A	N/A	N/A	N/A	1454.5 (27^{o})	N/A	N/A
1st critical angle (**practical**)	N/A	N/A	N/A	N/A	N/A	N/A	N/A	N/A	N/A	N/A	N/A	N/A
1st critical angle (**theoretical**)	12.44^{o}	8.97^{o}	32.41	12.3^{o}	9.0^{o}	30.98	11.02^{o}	11.96^{o}	8.18	5.09^{o}	5.71^{o}	11.48
2nd critical angle (**theoretical**)	30.59^{o}	29.5^{o}	3.63	30^{o}	31.5^{o}	4.88	28.7^{o}	30^{o}	4.43	32^{o}	31.5^{o}	1.57
2nd critical angle (**theoretical**)	N/A	N/A	N/A	N/A	N/A	N/A	N/A	N/A	N/A	N/A	N/A	N/A
Critical angle velocity prediction	1301.9	1344.4	3.21	1322.6	1266	4.37	1376.2	1321.4	4.06	1246	1263.54	1.39

4.0 DISCUSSION

Small % errors in wave velocity were found for both v-CFRP sample A and B, indicating a good degree of homogeneity between the samples. Further, the wave profile recorded for the samples was largely independent of incident angle and was indicative with that expected for an isotropic plane [14,17]. Thus, as verified via ultrasonic wave propagation the lay-up presented in this work provides a reasonable approximation for in plane isotropy.

The wave profile recorded for the rf-samples differed from that recorded for the v-CFRP in that the wave velocities were much more susceptible to incident angle. This was particularly true for transverse wave velocity, which decreased as the incident angle was approached. All rf-samples recorded a relatively similar pattern of wave propagation except from C1, this sample recorded two transverse waves, with one quickly attenuating at around 13.5^{o}. In this case a larger deviation, when compared to the other samples, away from isotropic symmetry was inferred with possible error arising from the rf-CFRP manufacturing process. Further, the degree of homogeneity between the samples was inferred via wave velocity; higher % errors than what was recorded in the case of v-CFRP

for longitudinal waves at 0^0 were found. Additionally, both the recycled and simulated recycled recorded the same wave profiles, indicating that on a macroscopic level the materials behaved very similar in terms of wave propagation. Table 5 provides a general comparison of findings between v-CFRP and rf-CFRP.

The focus of this work was to investigate if wave propagation for rf-CFRP differed in profile from that recorded from v-CFRP, given similar fiber architecture. The close relationship found in terms of critical angles, and wave profile suggests that both v-CFRP and rf-CFRP shared a good degree of similarity. Taking this into account and acknowledging varying velocity and amplitude values observed for the rf-CFRP samples, which underwent identical pyrolysis and manufacturing processes, we suggest that more severe changes in velocity with increasing incident angle for the rf-CFRP were most likely caused by a non-ideal resin impregnation process and that given identical resin fiber content for both v-CFRP and rf-CFRP a more closely related wave profile, in terms of velocity will be returned. This is no way infers that similar sample properties will be recorded; it is overwhelming the case that the elastic constants will differ for the rf-CFRP.

This hypothesis is limited to the composite under investigation in this research and has still to be verified and expanded upon by developing a more robust resin impregnation process. Moving forward, to develop a wider ranging and more fundamental understanding of wave propagation in rf-CFRP, when compared to similar v-CFRP, further investigation into areas such as group velocity effects, different fiber architectures, different types of fibers, different types of wave, residual resin, amplitude profile, attenuation profile, dwell times, fiber/resin adhesion problems, accuracy of elastic constant determination, sample geometry, recycling methods, manufacturing methods etc. is required.

TABLE 5. Comparison of experimental findings from application of ultrasound through transmission to v-CFRP and rf-CFRP

Data	V-CFRP	rf-CFRP (A1-D2)
Longitudinal wave speed	Remained largely constant	Mixed results
Transverse wave speed	decrease with increasing incident angle (% difference of 10-17)	decrease with increasing incident angle (% difference of 21-33)
Velocity variation between samples	Very small changes for both longitudinal and transverse waves	Large changes in longitudinal velocity but very small changes recorded for transverse waves
Amplitude variation between samples	Very small changes in wave amplitude	Mixed results with some cases of large change in wave amplitude
Amplitude profile	As expected from theory	Largely matched v-CFRP in every case bar C1
First critical angle	Not observable	Not observable
Second critical angle	32^0	$29\text{-}32^0$
Transverse critical angle velocity prediction (average)	1250 m/s	1305.18 m/s

5.0 CONCLUSION

A simple way to create relatively accurate quasi-isotropic CFRP was identified with the in-plane elastic constants identified via ultrasonic wave velocity measurements. Further, v-CFRP was recycled, with the resulting fibers used to manufacture rf-CFRP. The rf-CFRP samples recorded more anisotropy than the v-CFRP samples in that wave velocity decreased more severely with incident angle. Owing to the varying velocity, the elastic constants of the rf-CFRP were not able to be determined using the same equations as for the v-CFRP. The authors suggest that a more closely related wave profile for v-CFRP and rf-CFRP will be produced for the architecture outlined in this research, given similar resin fiber content. However, further investigation using a more robust resin impregnation process is required to verify this claim. Additional research areas were also identified to develop to allow for a better understanding of potential subtle differences recorded when investigating bulk wave propagation in rf-CFRP, when compared to v-CFRP

ACKNOWLEDGEMENTS

This work was performed with support from the Engineering and Physical Science Research Council (United Kingdom), EP/I015698/1.

6.0 REFERENCES

[1] Zimmer JE, Cost JR. Determination of the elastic constants of a unidirectional fiber composite using ultrasonic velocity measurements. Acoustical Society of America 1970;47:795–803.
[2] Markham MF. Measurement of the elastic constants of fiber composites by ultrasonics. Composites 1970;1:145–9.
[3] Rokhlin SI, Chimenti DE, Nagy PB. Physical Ultrasonics of Composites. Oxford university press; 2011.
[4] Pearson LH, Murri WJ. Measurement of ultrasonic wavespeeds in off-axis directions of composite materials. In: Thompson DO, Chimenti DE, editors. Review of Progress in Quantitative Nondestructive Evaluation, vol. 6A, Springer US; 1987, p. 1093–101. doi:10.1007/978-1-4613-1893-4_125.
[5] Rokhlin SI, Wang W. Double through transmission bulk wave method for ultrasonic phase velocity measurement and determination of elastic constants of composite materials. Acoustical Society of America 1992;91:3303–12.
[6] Hosten B. Ultrasonic through-transmission method for measuring the complex stiffness moduli of composite materials. In: Every AG, Sachse W, editors. Handbook of elastic properties of solids, liquids and gases, San Diego: Academic press; 2001, p. 67–86.
[7] Paterson DAP, Ijomah W, Windmill J. An analysis of end-of-life terminology in the carbon fiber reinforced plastic industry. International Journal of Sustainable Engineering 2016;9:130–40. doi:10.1080/19397038.2015.1136361.
[8] Pickering SJ. Recycling technologies for thermoset composite materials-current status. Composites Part A: Applied Science and Manufacturing 2006;37:1206–15. doi:10.1016/j.compositesa.2005.05.030.
[9] Pimenta S, Pinho S. Recycling carbon fiber reinforced polymers for structural applications: Technology review and market outlook. Waste Management 2011;31:378–92. doi:10.1016/j.wasman.2010.09.019.
[10] Pimenta S, Pinho S. The effect of recycling on the mechanical response of carbon fibers and their composites. Composite Structures 2012;94:3669–84. doi:10.1016/j.compstruct.2012.05.024.
[11] Oliveux G, Dandy LO, Leeke G a. Current Status of Recycling of Fiber Reinforced Polymers: review of technologies, reuse and resulting properties. Progress in Materials Science 2015;72:61–99. doi:10.1016/j.pmatsci.2015.01.004.
[12] Perry N, Bernard a., Laroche F, Pompidou S. Improving design for recycling - Application to composites. CIRP Annals - Manufacturing Technology 2012;61:151–4. doi:10.1016/j.cirp.2012.03.081.
[13] Pimenta S, Pinho ST, Robinson P, Wong KH, Stephen J. Mechanical analysis and toughening mechanisms of a multiphase recycled CFRP. Composites Science and Technology 2010;70,:1713–1725. doi:10.1016/j.compscitech.2010.06.017.
[14] Musgrave MJP. On the propagation of elastic waves in aeleotropic media:I General Principals. Proceddings of the Royal Society 1954;226:339–56. doi:10.1098/rspa.1954.0258.
[15] Musgrave MJP. On the propagation of elastic waves in aeleotropic media:II media of hexagonal symmetry. Proceddings of the Royal Society 1954;226:356–66. doi:10.1098/rspa.1954.0259.
[16] Miller GF, Musgrave MJP. On the propagation of elastic waves in aeolotropic media. III. Media of cubic symmetry. Proceddings of the Royal Society 1956;236:352–83. doi:10.1098/rspa.1956.0142.
[17] Auld BA. Acoustic fields and waves in solids, Volume 1. 2nd ed. Krieger publishing company; 1990.
[18] Prosser WH. Ultrasonic characterization of the nonlinear elastic properties of unidirectional graphite/epoxy composites. vol. October. 1987.
[19] Shi J, Kemmochi K, Bao LM. Research in Recycling Technology of Fiber Reinforced Polymers for Reduction of Environmental Load: Optimum Decomposition Conditions of Carbon Fiber Reinforced Polymers in the Purpose of Fiber Reuse. Advanced Materials Research 2012;343–344:142–9. doi:10.4028/www.scientific.net/AMR.343-344.142.
[20] Meyer LO, Schulte K, Grove-Nielsen E. CFRP-Recycling Following a Pyrolysis Route: Process Optimization and Potentials. Journal of Composite Materials 2009;43:1121–32. doi:10.1177/0021998308097737.

[21] Trogé A, O'Leary RL, Hayward G, Pethrick RA, Mullholland AJ. Properties of photocured epoxy resin materials for application in piezoelectric ultrasonic transducer matching layers. Acoustical Society of America 2016;128:2704–14. doi:10.1121/1.3483734.